On the effect of gravitational and hydrodynamic forces on particle motion in a quiescent fluid at high particle Reynolds numbers

M. Rostami, A. Ardeshir, G. Ahmadi, and P.J. Thomas

Abstract: Trajectories of 5 and 10 mm metallic and plastic particles in a quiescent liquid during their sedimentation toward a plate were studied using experimental and numerical means, and the influence of gravity, drag, added mass, and history forces were evaluated. Variations of particle diameter and density allowed measurements at Reynolds numbers, based on the impact velocity, in the range of 1 000 to 13 000. A computer model was developed and the Lagrangian equation of particle motion was solved. The results showed that the combination of gravity, drag, and added mass forces are important for the simulation of the motion of small particles for the duration of their flight from the starting point to the wall impact, in the range of particle Reynolds numbers between 1000 and 5000. Comparison of the simulation results with the data showed that the predicted trajectories underestimated the experimental observations by about 1% to 4.3%. When the history force was included in the governing equation, however, excellent agreement between the measured and predicted particle trajectory was obtained. Experimental results for the motion of large particles showed oscillations in the time history of particle velocity when the particle Reynolds number was in the range of 3 000 to 13 000. Repeating the experiment, and averaging the data of a large number of experiments, yielded averaged curves for the particle velocity that did not show oscillatory values. In this case, good agreement between numerical and experimental data was observed. The study also shows that at high particle Reynolds numbers, the effect of the history force becomes negligibly small.

PACS No.: 47.55kf

Résumé : Nous étudions expérimentalement et numériquement les trajectoires de particules de plastique et de métal de 5 et 10 mm dans un liquide au repos pendant leur sédimentation vers une plaque et évaluons l'influence de la gravité, de la résistance hydrodynamique de la masse ajoutée et des forces de Boussinesq. Variant le diamètre et la densité des particules et mesurant la vitesse d'impact nous a permis de déterminer des valeurs du nombre de Reynolds entre 1 000 et 13 000. Nous avons développé un modèle numérique et solutionné les équations de mouvement de Lagrange. Les résultats montrent que la gravité, la résistance et la masse ajoutée ont un effet important dans la simulation du mouvement des petites particules pendant leur trajectoire entre le point de départ et l'impact sur le mur, pour un nombre de Reynolds entre 1000 et 5000. La comparaison avec les observations montre que les simulations sous-estiment les trajectoires par 1 à 4,3 %. L'ajout des forces de Boussinesq permet alors aux trajectoires calculées d'être en excellent accord avec les trajectoires observées. Les expériences avec des particules plus grosses ont montré des oscillations dans l'évolutions temporelle de la vitesse, lorsque le nombre de Reynolds était entre 3 000 et 13 000. En répétant les expériences et en prenant la moyenne sur un grand nombre d'expériences nous obtenons des trajectoires moyennes sans oscillations de la vitesse. Dans ce cas, nous avons un bon accord entre les simulations et les trajectoires moyennes. L'étude montre aussi que l'effet des forces Boussinesq devient négligeable pour des nombres de Reynolds importants.

[Traduit par la Rédaction]

1. Introduction

The accurate evaluation of the hydrodynamic forces acting on a particle moving in a viscous fluid remains a fundamental question in multiphase flow modeling. This need arises in many engineering applications, for example, computer simulations of spray combustion, pollution control, boiling and bubble dynamics, sedimentation, and erosion of turbine blades. All these problems are concerned with the interaction of particles with fluids, which requires accurate knowledge of all hydrodynamic forces acting on a particle. Another area of interest is associated with the ability of dispersed solid particles to follow the fluid motion when their density or initial velocity does not match the fluid velocity or its density; that is, the ability of solid particles to behave as tracers of fluid motion. This issue is of importance for the prediction of dispersion of particles in flows, as well as for measurement techniques such as particle image velocimetry (PIV). Another motivation comes from work aimed at developing a Lagrangian tracking technique for the motion of solid

Received 16 June 2006. Accepted 30 October 2007. Published on the NRC Research Press Web site at http://cjp.nrc.ca/ on 19 June 2008.

M. Rostami[1] **and A. Ardeshir.** Department of Civil and Environmental Engineering, AmirKabir University of Technology, Tehran, Iran.
G. Ahmadi. Department of Mechanical and Aeronautical Engineering, Clarkson University, 8 Clarkson Ave., Potsdam, NY 13699, USA.
P.J. Thomas. Department of Engineering, University of Warwick, Coventry, UK.

[1]Corresponding author (e-mail: m_rostami@aut.ac.ir).

 doi: 10.1139/P07-198

particles over large time intervals. It raises the question of the response of a particle to rapid changes in the velocity of the fluid or to a sudden acceleration. Analytical approaches to the time-dependent motion of a solid particle in a given quiescent fluid have been restricted to zero or small-particle Reynolds numbers. However, they provide a general framework for the description of the forces acting on the particle.

The equation of particle motion in its general form is rather cumbersome to deal with. Usually, various simplified versions are used. In most available models, among the forces acting on a particle, the gravity or buoyancy force, the quasi-steady drag, and the added mass force are included and their adequate expressions are now well-defined. The history force, which accounts for the vorticity diffusion in the surrounding fluid and the disturbance effect caused by the acceleration of the sphere, is often neglected in simulations of particle trajectory. The importance of the history term in the equation of particle motion still needs to be clarified. If one considers the equation of the particle motion trajectory with parameters corresponding to the creeping flow approximation, one finds that the history force may become important in certain situations.

In several papers, advection of particles with inertia in a fluid was investigated numerically under an assumption that the history force can be neglected [1–8]. Ounis and Ahmadi [9] studied the motion of small spherical particles in a random flow field. The Stokes drag, virtual mass, and the Basset (history) forces were included in their equation of particle motion. Results obtained recently for the motion of particles in supersonic flow across oblique shocks showed that the Basset force could be even more significant than the Stokes drag force [10]. Abbad et al. [11, 12] did experiments to study a free-falling rigid sphere in a quiescent incompressible Newtonian fluid, placed in an oscillating frame. They investigated, numerically, the effect of the history force acting on the sphere at small-particle Reynolds numbers ($\mathrm{Re_p} \leq 2.5$). The comparison was made by solving the equation of motion for the sphere with and without the history force. They found that the history force plays a significant role in the momentum balance. Harada et al. [13] studied, both experimentally and numerically, a spherical nylon particle of diameter 12.7 and 25.4 mm approaching a wall in an incompressible fluid under the action of gravity at particle Reynolds numbers 6.01 and 25.8, respectively. Their results showed that in addition to the gravity, the drag, and the added mass force, the Basset history force also had a significant effect on the particle motion through the sedimentation in both cases. Gondret et al. [14] investigated, both experimentally and numerically, the bouncing motion of solid spheres onto a solid plate in an ambient fluid. They demonstrated that the history force cannot be neglected for the bouncing trajectories after the collisions, for particle Reynolds numbers up to about 10^3.

Most of the previous studies have been performed on the motion of particles in a quiescent fluid at low or moderate particle Reynolds number.

The objective of the present paper is to examine the effect of hydrodynamic forces on the motion of spherical metallic and plastic particles of different diameters at large particle Reynolds numbers ($\mathrm{Re_p} > 1000$). Both experiments and numerical analyses were conducted to examine the fluid-forces model for a range of particle Reynolds number between 1 000 and 13 000. The particle trajectories from their initial rest position to the wall impacts were examined. Spheres of different densities and diameters were used in the experimentation. The particle trajectories were also calculated using a Lagrangian method. The equation of particle motion included gravity, drag, added mass, and history forces with proper modification. To assess model validation, the numerical simulations were compared with the experimental data and with available results from other researchers.

2. Formulation and numerical method

The particle trajectory can be determined by solving the corresponding governing equation of motion, which can be deduced from Newton's Second Law. The equation of motion for small particles in a viscous quiescent fluid dates back to the pioneering work of Basset, Boussinesq, and Oseen, and is commonly known as the BBO equation. They solved the Navier–Stokes equations for a creeping flow by neglecting the advective acceleration terms and derived the following equation for the motion of a sphere in a quiescent viscous fluid [15]:

$$m_\mathrm{p}\frac{\mathrm{d}\upsilon_\mathrm{p}}{\mathrm{d}t} = -6a\pi\mu_\mathrm{f}\upsilon_\mathrm{p}\varphi - \frac{1}{2}m_\mathrm{f}\frac{\mathrm{d}\upsilon_\mathrm{p}}{\mathrm{d}t} + \left(m_\mathrm{p} - m_\mathrm{f}\right)g - 6a^2\sqrt{\pi\mu_\mathrm{f}\rho_\mathrm{f}}\int_0^t \frac{\mathrm{d}\upsilon_\mathrm{p}/\mathrm{d}t}{\sqrt{t-\tau}}\mathrm{d}\tau \quad (1)$$

where ρ_f is the density of the fluid, μ_f its viscosity, υ_p is the sphere velocity, a its radius, m_p its mass, and m_f is the mass of the fluid displaced by the sphere ($m_\mathrm{f} = (4/3)\pi a3\rho_\mathrm{f}$). The right-hand side of (1) consists of the summation of all forces exerted on the particle along its trajectory in a quiescent fluid. The terms on the right-hand side of (1) are, in the order of their appearance, steady drag (F_D), virtual mass force (F_A), gravity force (F_G), and Basset history force (F_H).

The steady drag is responsible for the terminal velocity of a sphere falling under gravity. The expression in (1) is only valid for very small $Re_\mathrm{p} = 2a\rho_\mathrm{f}\upsilon_\mathrm{p}/\mu_\mathrm{f}$ [16]. It is well known that for finite-particle Reynolds numbers, the convective inertia increases the drag. The analytic expression is not known for large-particle Reynolds numbers, but the empirical law for the drag coefficient as a function of Re_p is well documented for values of Re_p up to 3×10^7. One usually writes the steady drag as [16],

$$F_\mathrm{D} = -6a\pi\mu_\mathrm{f}\upsilon_\mathrm{p}\varphi \quad (2)$$

where φ is a function of the particle Reynolds number. Various approximations of $\varphi(Re_\mathrm{p})$ for rigid spherical particles can be found in the book by Clift et al. [16]. In the present study, we used the following approximation of the $\varphi(Re_\mathrm{p})$, valid for a wide range of particle Reynolds numbers [17],

$$\varphi = \left(1 + 0.15\,Re_\mathrm{p}^{0.687}\right) + \frac{1.75 \times 10^{-2}\,Re_\mathrm{p}}{1 + 4.25 \times 10^4\,Re_\mathrm{p}^{-1.16}} \quad \forall\, Re_\mathrm{p} < 3 \times 10^5 \quad (3)$$

Odar and Hamilton [18] and Odar [19] studied experimentally the force on a guided sphere rectilinearly oscillating in an otherwise stagnant fluid. They proposed an equation for the motion

Fig. 1. Components of the experimental set-up.

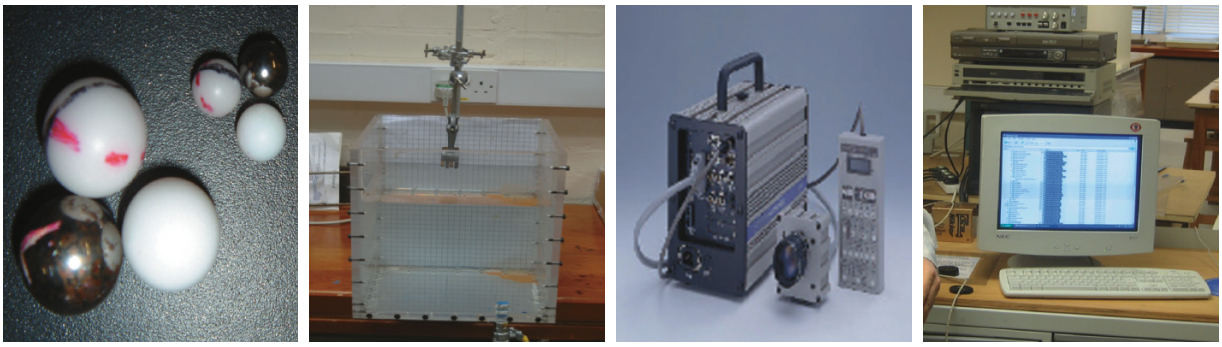

(a) Particles (b) Plexiglas tank (c) High Speed camera (d) Computer

Table 1. Properties of the particles used in the experiments.

Particle type	ρ_p/ρ_f	d (mm)	Falling height h_o (mm)	Impact velocity U_i (m/s)	Bed impact time t_i (s)	Re_p ($dU_i\rho_f/\mu_f$)	Remarks
Delrin®	1.362	5	195.5	0.215	1.02	1073	Used in this study
	1.362	10	195.5	0.333	0.808	3 330	Used in this study
Teflon®	2.304	5	195.5	0.409	0.566	2 043	Used in this study
	2.304	10	195.5	0.560	0.464	5 590	Used in this study
Steel	7.794	5	195.5	1.049	0.273	5 235	Used in this study
	7.794	10	195.5	1.221	0.252	12 190	Used in this study
	7.822	3	500	0.810	0.649	2 700	Ref. 21
	7.721	4	500	0.970	0.597	4 300	Ref. 21

of a sphere based on their experimental study as,

$$m_p\frac{d\upsilon_p}{dt} = -6a\pi\mu_f\upsilon_p\varphi - \frac{1}{2}C_a m_f\frac{d\upsilon_p}{dt} + \left(m_p - m_f\right)g - 6a^2C_h\sqrt{\pi\mu_f\rho_f}\int_0^t\frac{d\upsilon_p/dt}{\sqrt{t-\tau}}d\tau \quad (4)$$

with C_a and C_h are obtained experimentally and given by,

$$C_a = 2.1 - \frac{0.132}{A_c^2 - 0.12} \quad (5)$$

$$C_h = 0.48 - \frac{0.32}{(A_c+1)^3} \quad (6)$$

The parameter A_c is called the acceleration number and is defined by

$$A_c = \frac{2\upsilon_p^2}{a\left|d\upsilon_p/dt\right|} \quad (7)$$

Note that in the inviscid limit, the added mass force is modified by the presence of a wall by the factor $(1 + 3a^3/8(a+h)^3)$, where h is the distance of the bottom apex of the particle to the wall [20].

In this paper, for simulating the particle trajectories a numerical model based on (4) was developed. The velocity of a particle is obtained by integrating (4) using the Runge–Kutta fourth-order method, and the particle position is determined according to the velocity ($\upsilon_p = dx/dt$). In the numerical simulation, the main problem in solving (4) is the history force term. To solve this problem, it is assumed that the general temporal variation of particle velocity can be broken up into a series of step changes. At time 0 there is a change $\Delta\upsilon_{p0}$, at time t_1 a change $\Delta\upsilon_{p1}$, at time t_2 a change $\Delta\upsilon_{p2}$, and so on. For instance, to compute the effect of the history force at time t_3, the cumulative effect of the history force can be written as follows [17]:

$$F_{H_{(t_3)}} = 6a^2C_h\sqrt{\pi\mu_f\rho_f}\int_0^{t_3}\frac{d\upsilon_p/dt}{\sqrt{t-\tau}}d\tau = 6a^2C_h\sqrt{\pi\mu_f\rho_f} \times\left[\frac{\Delta\upsilon_{p0}}{\sqrt{t_3}} + \frac{\Delta\upsilon_{p1}}{\sqrt{t_3-t_1}} + \frac{\Delta\upsilon_{p2}}{\sqrt{t_3-t_2}}\right] \quad (8)$$

3. Experimental set-up

The trajectory of solid particles falling toward a Plexiglas® plate was investigated experimentally. Components of the experimental set-up are shown in Fig. 1. We used solid spheres made of different materials (Delrin®, Teflon®, and steel) and of different diameters. Their specifications and main characteristics of motion are summarized in Table 1. The experiments were conducted by dropping the particles in water in a rectangular Plexiglas® tank with base dimensions of 275 mm × 275 mm and a depth of 280 mm. The mass density of the water was 998.1 kg/m^3, and the viscosity was 1×10^{-3} Pa s (at $T = 20°$). To avoid air contamination, the particles were initially submerged and held in a place a few millimetres under the water surface by means of a suitable support. The particle

Fig. 2. Sample pictures of the 5 mm particles dropped from a height of 0.195 m onto the Plexiglas® plate.

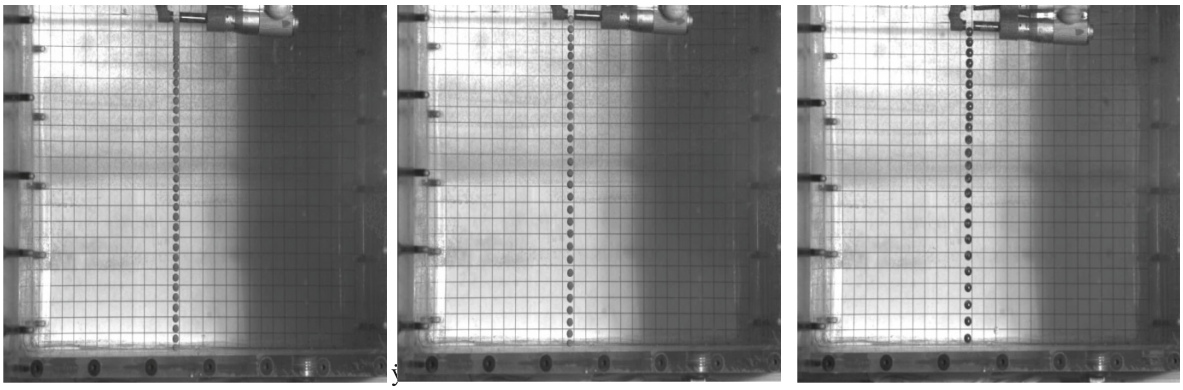

(a) Delrin (b) Teflon (c) Steel

trajectory is recorded by a high-speed camera (Photron Fastcam PC1 1024) at 1000 frames/s. The recorded sequences of the particle motion are analyzed by using the Photron Fastcam viewer (PVF).

4. Results

In this section, we compute the particle trajectory numerically and compare the results obtained with the experimental data.

Figure 2 depicts a series of sequences of photographs of the 5 mm particles of different materials as they fall toward the Plexiglas® plate. From these pictures, the instantaneous particle displacement was evaluated using the PVF software. The computational model allows us to add or omit any of the exerted forces (F_G, F_D, F_A, and F_H) so that the influence of different forces can be studied. Figure 3 compares the experimental and simulated position of the Delrin® sphere of diameter 5 mm at different times. Here, the simulations were performed for various combinations of the exerted hydrodynamic and gravitational forces. Figure 3 shows that the time duration for the particle to impact the bed ($T = 0.382$ s), when the numerical model neglects the hydrodynamic forces and only includes gravity (F_G), is 0.375 of that observed in the experiment ($T = 1.02$ s). Figure 3 also shows that the time-to-impact ratio (simulation to experiment) increases to about 0.92 when, in addition to gravity F_G, the drag force, F_D, is taken into account. This ratio becomes 0.95 when the apparent mass effect F_A is also included in addition to F_G and F_D. When the Basset history force F_H is also included in the computer model, Fig. 3 shows very good agreement between the simulated time to impact with that of the experiment. In this case, the particle Reynolds particle number (Re_p), based on the impact velocity (U_i) is found to be about 1073. Therefore, Fig. 3 implies that neglecting the history force leads to about 5% discrepancy between the numerical simulation and experimental data.

Figure 4 compares the experimental data with simulated trajectories of the 5 mm Delrin® sphere as predicted by different models. Figure 4 shows detailed information on the effect of various hydrodynamic forces on the motion of the Delrin® particle. Clearly the drag force is the dominant force, but the apparent mass and the history forces have small but noticeable effects. Here again, an excellent agreement with experimental data is observed when all the hydrodynamic forces, including the history force, are included in the computational model. In this case, detailed examinations of the numerical results show that the gravity, drag, added mass, and history forces have a contribution equal to 52.9%, 34.7%, 8.1%, and 4.3% , respectively, on the motion of the particle toward the plate. Figure 5 compares the temporal variation of the predicted particle velocities with the experimental data. The influence of the hydrodynamic forces on the motion of the Delrin® particle can clearly be seen from Fig. 5. These curves provide clear information about the effect of different hydrodynamic forces on the motion of the Delrin® particle. Here, an excellent agreement is observed when the history force is included in the computer model.

By choosing the Teflon® particle of diameter 5 mm and changing the value of density from 1360 to 2300 kg m^{-3}, we vary the ratio of inertia to gravitational mass. It is then expected that the motion of a heavier bead (Teflon®) to be less influenced by the eventual unsteadiness of its wake. Figure 6 shows the trajectory and velocity profile of the Teflon® sphere. As is evident from Fig. 6, when only the gravity (F_G) and the drag force (F_D) are taken into account, the simulation approaches up to about 89.7% of the experimental data. With the addition of the added mass (F_A) force, the accuracy of the simulation results increase up to about 97.0%. However, there is still a 3% discrepancy between the experimental and numerical results. When the history force (F_H) is also included, the simulation results are in excellent agreement with the experimental data. In this case $Re_p \approx 2043$.

The steel beads were tested in the experiment for increasing particle Reynolds numbers. Figure 7 compares the experimental and numerical trajectories and the time history of particle velocities for the 5 mm steel sphere at $Re_p \approx 5235$ in water. Figure 7 shows that when the history force (F_H) in (4) is neglected, the simulation results are in reasonable agreement with the experimental data. A detailed examination of the simulation results shows that the history force contributes about 1%.

Equation (4) shows that the effect of particle size on the history force increases with the square of radius (a^2). Thus, by increasing the particle size from 5 to 10 mm for the same density, we expect the motion of the bigger beads to be more influenced by the eventual unsteadiness of their wake. Figure 8 depicts the sequences of snapshots of the 10 mm particles movement toward the Plexiglas® base plate in water. It is seen that the path

Fig. 3. Comparison of computed position of the 5 mm Delrin® particle with the experimental data.

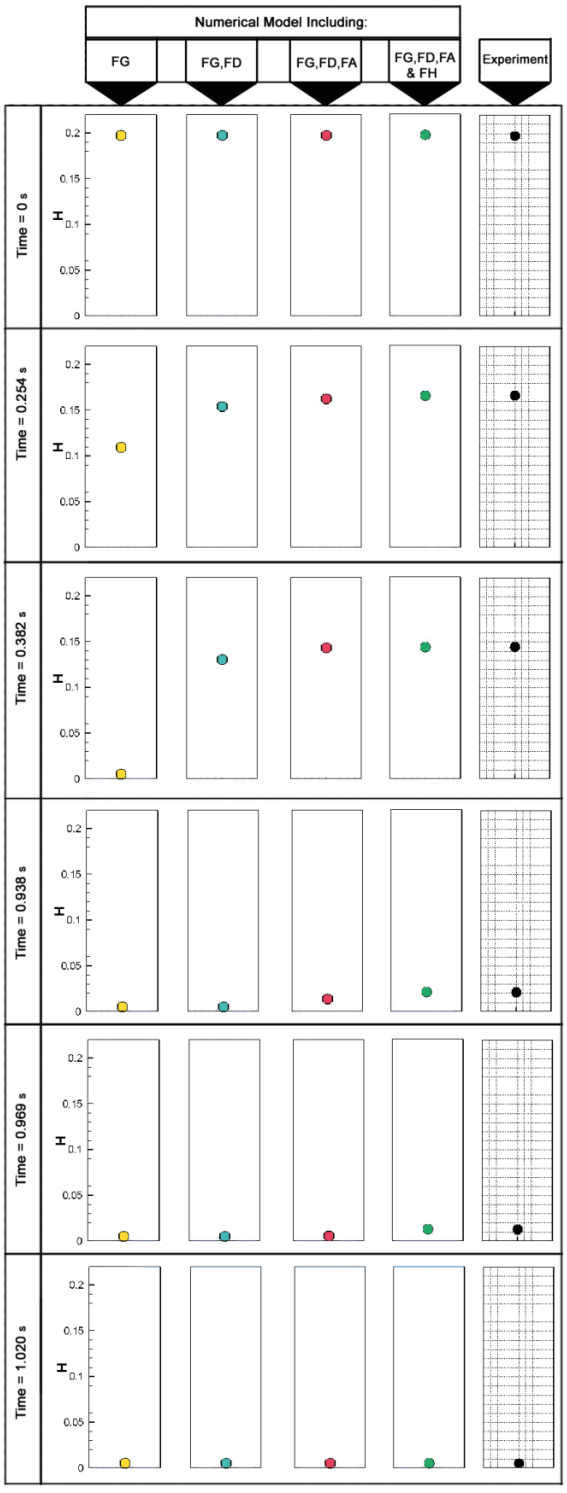

of the particle deviates from a straight line. To provide an understanding of the behavior of these particles, the instantaneous velocity of the particles were extracted from these experiments.

In Fig. 9, the markers (crosses) identify the velocity of particles 10 mm in diameter and different materials for a single run of the experiment. As Fig. 9 shows, the velocity presents oscillations while approaching its terminal value. However, we note

Fig. 4. Comparison of the trajectories of the 5 mm Delrin® particle, as predicted with different models, with the experimental measurements.

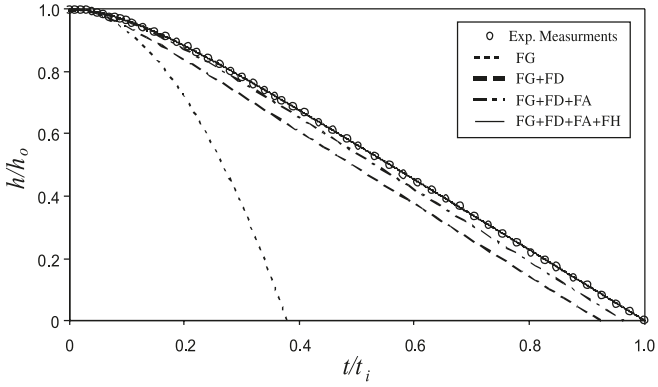

Fig. 5. Temporal variations of particle velocity for the motion of Delrin® particle in water, as predicted by different models, compared with the experimental data.

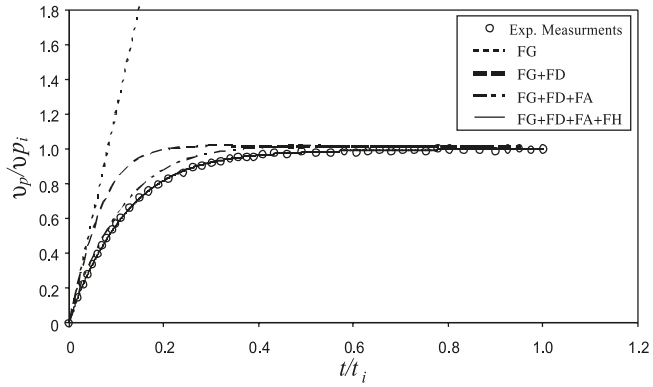

that the oscillations for the steel particle are smaller than what is reported for the Delrin® and Teflon® particles. Such oscillations must be linked to a temporal evolution of the particle wake. One observes that the velocity is no longer a monotonous function of time; it alternates between periods of increase and decrease. For this to happen, the acceleration of the particle must change sign; in particular the reaction of the wake on the particle is sufficient to overcome the gravitational force. Note that the particle Reynolds number is close to 3330, 5590, and 12 190 for the Delrin®, Teflon®, and steel particles, respectively. In this study, two other experiments for each particle were conducted and the data from all three experiments were averaged. As Fig. 9 shows, the oscillations nearly disappear if the motion is averaged over three falls (broken line).

From Fig. 9, the vanishing of the oscillations when averaging implies that the events in the wake that are responsible for them are not coherent, in the sense that they do not occur at fixed times. It is tempting to associate these events with the vortex shedding that may occur at these particle Reynolds numbers for the large particles. It should be noted that this is not observed for the small spheres ($d = 5$ mm).

Figure 10 shows the experimental and numerical velocity profile of the particles with 10 mm diameter. As revealed by Fig. 10, the numerical model (includes F_G, F_D, F_A, and F_H) can predict the averaged velocity profile of the particle, coinciding with experimental observation.

Fig. 6. Comparison of the trajectories and velocities of the 5 mm Teflon® particle, as predicted with different models, with the experimental measurements. (*a*) Trajectory and (*b*) velocity.

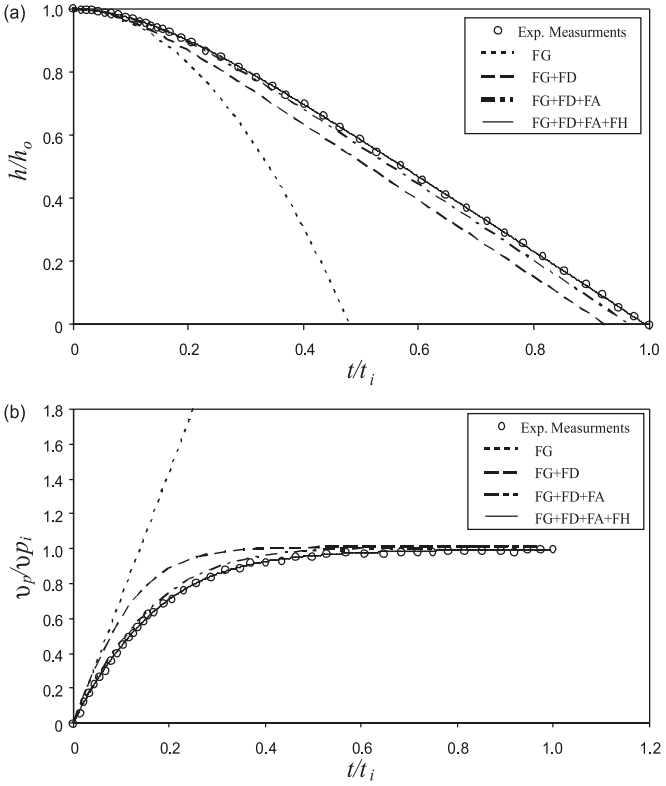

Fig. 7. Comparison of the trajectories and velocities of the 5 mm steel particle, as predicted with different models, with the experimental measurements. (*a*) Trajectory and (*b*) velocity.

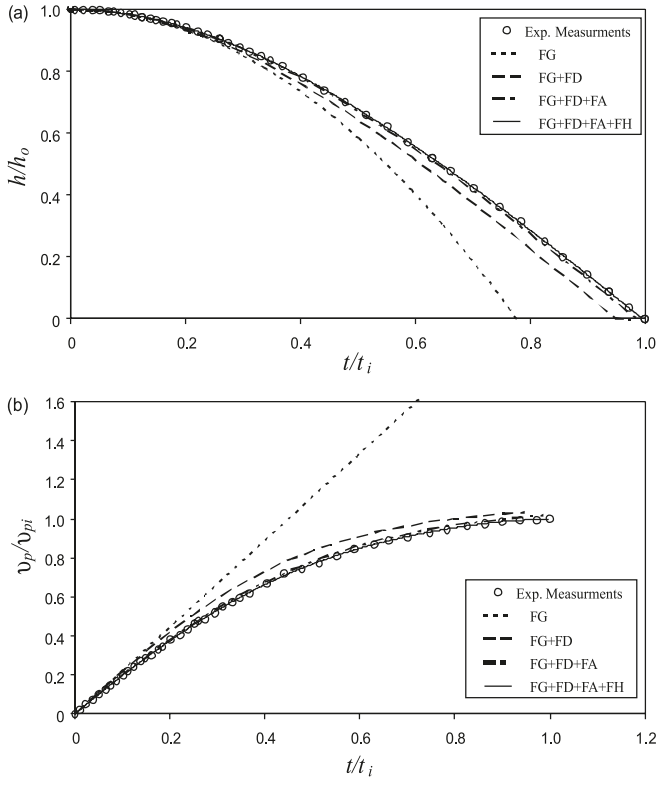

Fig. 8. A sample picture of the 10 mm particle dropped from a height of 0.195 m onto the Plexiglas® plate.

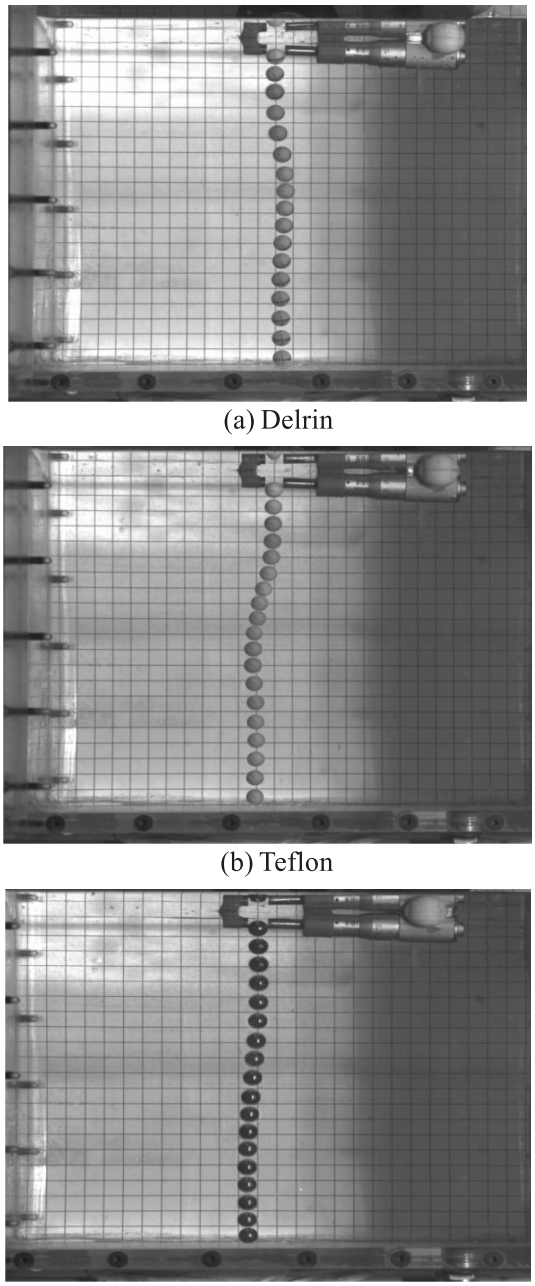

Figure 11 summarizes the contribution of each hydrodynamic force as obtained from the numerical simulations of the particle trajectories with respect to the particle Reynolds number (Fig. 11). The results of the numerical model for the motion of particles with Reynolds number between 1 000 and 13 000 indicate that in addition to gravity force (F_G), the drag force (F_D) is the dominant contribution, especially for the light particles. The third most important contribution in increasing the accuracy of the model compared with observations is the apparent mass force, while the history force (F_H) yields the smallest contribution to the final result.

Finally, the numerical calculations from our model (including F_G, F_D, F_A, and F_H) for the motion of steel particles of

Fig. 9. Velocity measurement, without averaging, for the 10 mm spheres.

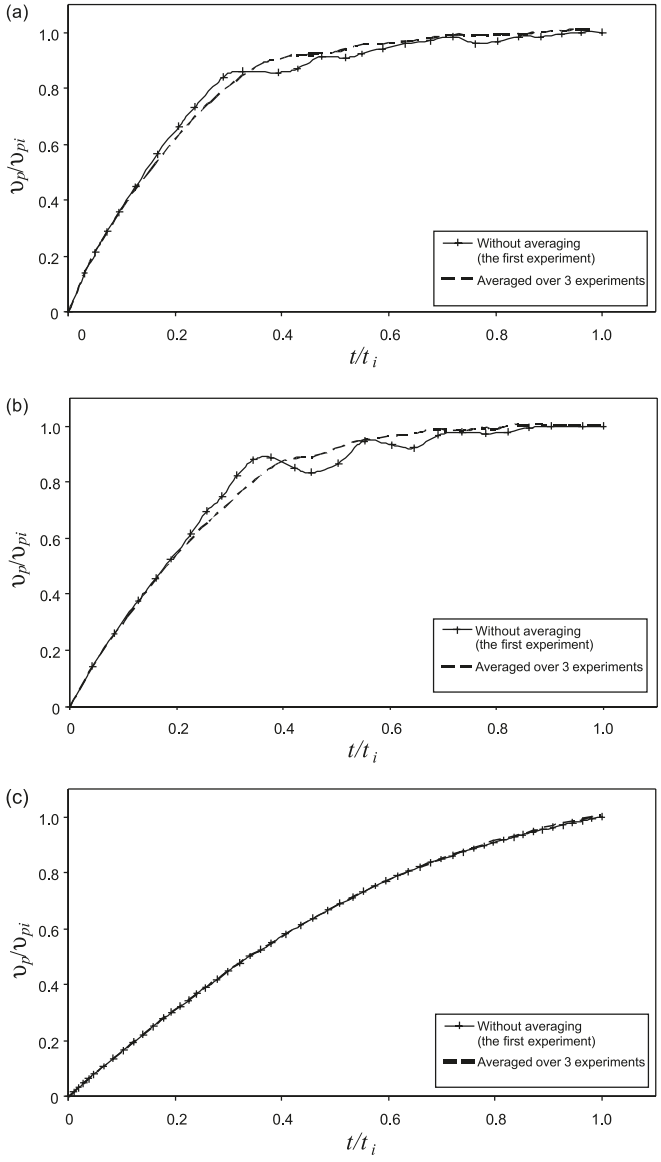

Fig. 10. Experimental and numerical results of the velocity profile for the motion of the 10 mm (*a*) Delrin®, (*b*)Teflon®, and (*c*) steel particles.

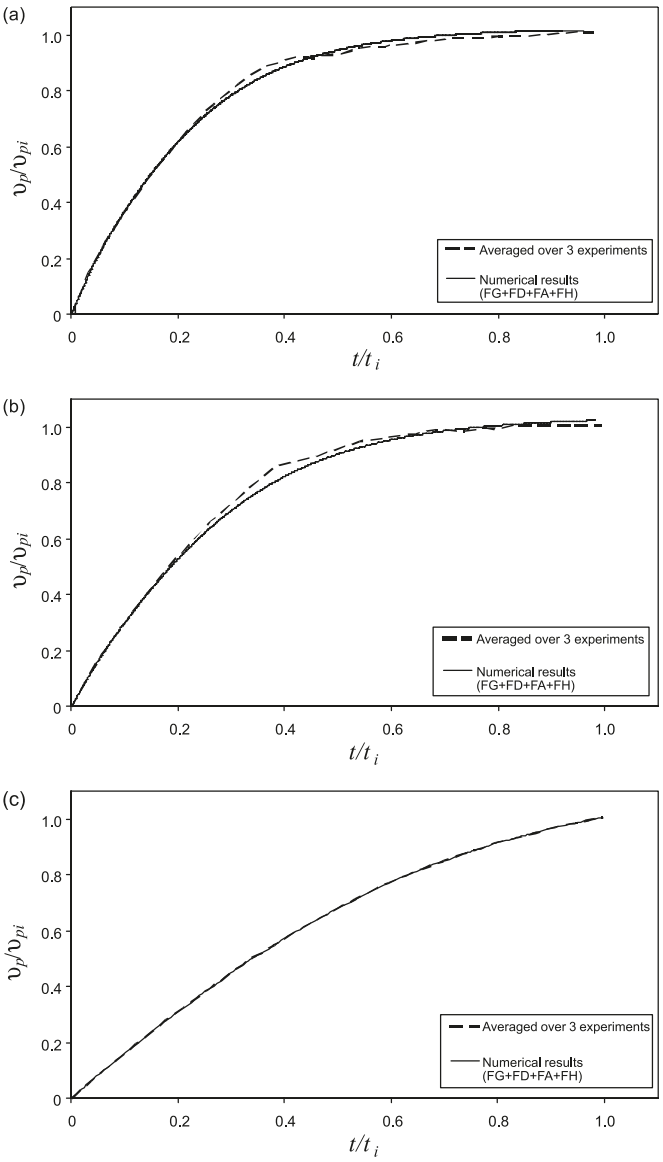

diameter 3 and 4 mm in water are compared with the experimental data of Mordant and Pinton [21]. Figure 12 reveals good agreement between the numerical and the experimental results, corroborating the high accuracy of the present model at high particle Reynolds numbers.

5. Conclusion

In the literature there are many experimental studies on the effect of hydrodynamic forces acting on macroscopic particle motion at low and moderate particle Reynolds numbers [10–14]. This prompted us to investigate, numerically and experimentally, how each hydrodynamics force affects the particle motion at high particle Reynolds numbers. To this end, experiments were carried out to study the free motion of spherical particles of 5 and 10 mm diameters and different material (Delrin®, Teflon®, and steel) in water during their sedimentation toward a plate. Variation of the sphere size and density allowed measurements at particle Reynolds numbers, based on the terminal velocity, between 1 000 and 13 000. By using a video-tracking technique and image processing, accurate measurements of the particle position and velocity were carried out. This study showed that in water and with the 5 mm particles, taking only gravity into account leads to an underestimate of the particles trajectory. The dissipating role of the drag force is important in explaining the trajectory but not sufficient, and the added mass effect turns out to be non-negligible even for a density ratio of about 7. However, the addition of these terms is not sufficient to reproduce the experimental curve, which clearly shows that the history force is necessary to predict correctly the particle trajectory. In this study, for the smaller particles, the addition of the drag force to gravity explained up to about 91% of the experimental curve. When the added mass force was included, then the accuracy of the simulation results increased up to about 97%. As a result, only about 3% of the results were

Fig. 11. Contribution of each force on the prediction of the correct trajectory of different particles with respect to the particle Reynolds number.

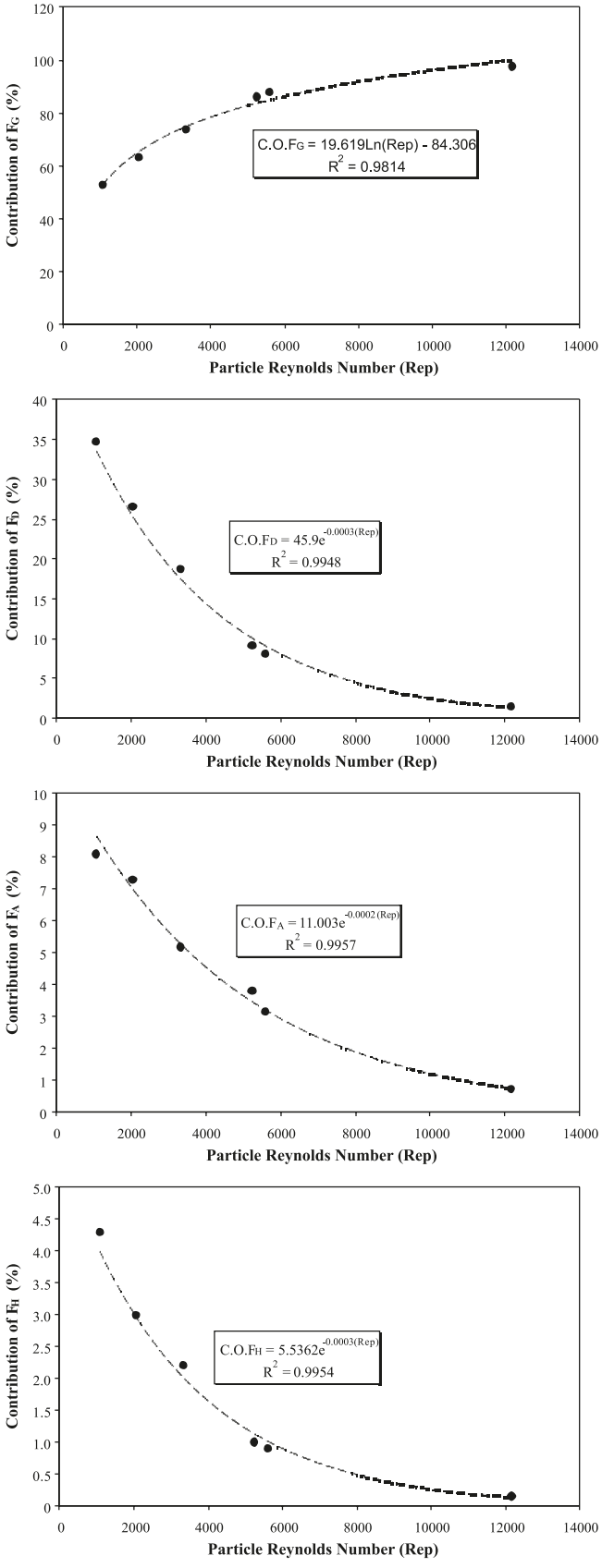

Fig. 12. Velocity profiles of the motion of steel particles in water at rest. The numerical results of (4) are compared with the experimental data of ref. 21.

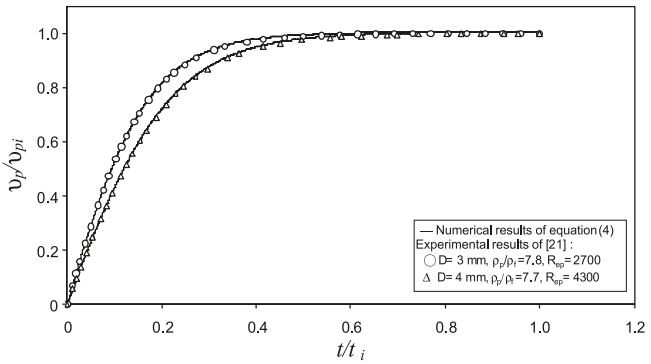

associated with the history force. It should be noted that for the smaller particles, the particle Reynolds number was between 1000 and 5000.

For the particles of 10 mm diameter, we observe a behavior not yet described by the numerical model (including F_G, F_D, F_A, and F_H), the velocity of the particle shows transitory oscillations while reaching a stationary limiting value. We propose that this may be due to transient vortex shedding in the wake of the large sphere at Reynolds numbers between 3 000 to 13 000, which affects and modifies the motion of the particle. Repeating the experiment and averaging the data of three runs yielded averaged curves for the particle velocity that did not show oscillatory values. These averaged curves were in good agreement with our numerical results. This indicates that for increasing particle Reynolds number the effect of the history force becomes weaker and can be ignored.

It is noted that throughout this study the influence of the particle on the fluid motion was assumed to be negligible (one-way coupling model). While this assumption appears to hold for both the small and large particles tested, our numerical model should be improved by including the effect of particles on the fluid, i.e., developing a two-way coupling model.

Acknowledgments

The first author acknowledges the financial support given by the Ministry of Education of the Islamic Republic of Iran and all the support offered by the Engineering Department of University of Warwick, UK. The first author is also particularly indebted to Graham Canham who assisted with the photography.

References

1. G. Barnoky and R.H. Davis. Phys. Fluids, **31**, 1324 (1988).
2. R.M. Brush, H.W. Ho, and B.C. Yen. J. Hydraulic Division, ASCE, Vol. 90, HY1, Proceeding paper 3764, 1964.
3. S.D. Gruttola, K. Boomsma, D. Poulikakos, and Y. Ventikos. Artif. Organs, **29**, 665 (2005.)
4. Z. Hu, X. Luo, and K.H. Luo. Theor. Comput. Fluid Dyn. **15**, 403 (2002).
5. W. Ling, J.N. Chung, T.R. Troutt, and C.T. Crowe. J. Fluid Mech. **358**, 61 (1998).
6. C. Marchioli and A. Soldati. J. Fluid Mech. **468**, 283 (2002).

7. N. Raju and E. Meiburg. Phys. Fluids, **9**, 299, (1997).
8. Q. Wang, K.D. Squires, and L.P. Wang. Phys. Fluids, **10**, 1700 (1998).
9. H. Ounis and G. Ahmadi. Trans. Am. Soc. Mech. Eng. **112**, 114 (1990).
10. P.J. Thomas. Phys. Fluids A, **4**, 2090 (1992).
11. M. Abbad, O. Caballina, and M. Souhar. Memory effect on spherical particles at low and intermediate Reynolds numbers. Advances in the modeling methodologies of two-phase flows. Lyon, France. 2004.
12. M. Abbad, O. Caballina, and M. Souhar. Phys. Fluids, **16**, 3808 (2004).
13. S. Harada, T. Tanaka, and Y. Tsuji. Fluid force acting on a falling particle toward a plane wall. *In* Proceedings 2000 ASME FEDSM'00. 11–15 June 2000. Boston, Mass. ASME, Mass. 2000.
14. P. Gondret, M. Lance, and L. Petit. Phys. Fluids, **14**, 643 (2002).
15. C.-M. Tchen. Ph.D. thesis. Delft University of Technology, the Netherlands. 1947.
16. R. Clift, J.R. Grace, and M.E. Weber. Bubbles, drops, and particles. Academic Press, New York. 1978.
17. C. Crowe, M. Sommerfeld, and Y. Tsuji. Multiphase flows with droplets and particles. CRC Press, Boca Raton, Fla. 1998.
18. F. Odar and W.S. Hamilton. J. Fluid Mech. **18**, 302 (1964).
19. F. Odar. J. Fluid Mech. **25**, 591 (1966).
20. L. Millne-Thomson. Theoretical hydrodynamics. MacMillan Education, London, UK. 1968.
21. N. Mordant and J.-F. Pinton. Eur. Phys. J. B, **18**, 343 (2000).